第33卷第2期
2014年4月

红外与毫米波学报
J. Infrared Millim. Waves

Vol. 33, No. 2
April, 2014

文章编号:1001-9014(2014)02-0122-07

DOI:10.3724/SP.J.1010.2014.00122

Multiframe registration based adaptive nonuniformity correction algorithm for infrared focal plane arrays

REN Jian-Le[1,2,3*], CHEN Qian[1,3], QIAN Wei-Xian[1], GU Guo-Hua[1], YU Xue-Lian[1], LIU Ning[1]

(1. Jiangsu Key Laboratory of Spectral Imaging & Intelligent Sense, Nanjing University of Science and Technology, Nanjing 210094, China;
2. Department of Computer Science, University of California, Davis, California 95616, USA;
3. Key Laboratory of Photoelectronic Imaging Technology and System, Ministry of Education of China, Beijing Institute of Technology, Beijing 100081, China)

Abstract: A novel adaptive scene-based nonuniformity correction method for fixed-pattern noise removal was put forward. It is based on the multiframe registration and estimation of global translation between several adjacent frames. The resulting mean square error function was optimized making use of the least mean square algorithm. Combining the local variance of an error function with the correlation peak value, the convergence speed can be controlled adaptively. The proposed method takes advantage of the correlation of adjacent frames sufficiently, thus it can provide enhanced results for diverse simulated and real infrared image sequences with nonuniformity. The experimental results show that the accurate estimations of the nonuniformity parameters of each detector in a focal plane array speed up the convergence, meanwhile, retain few ghosting artifacts.

Key words: infrared focal plane array, nonuniformity correction, least mean square, multiframe registration

PACS:42.30.Wb

基于多帧配准的红外焦平面阵列非均匀性自适应校正

任建乐[1,2,3*], 陈 钱[1,3], 钱惟贤[1], 顾国华[1], 于雪莲[1], 刘 宁[1]

(1. 南京理工大学 江苏省光谱成像与智能感知重点实验室,江苏 南京 210094;
2. 加利福尼亚大学 戴维斯分校 计算机科学与技术系,美国 加利福尼亚 95616;
3. 北京理工大学 光电学院 光电成像技术与系统教育部重点实验室,北京 100081)

摘要:提出了一种场景自适应的非均匀性校正固定图案噪声去除方法.基于多帧配准和相邻帧之间的全局位移估计,利用最小均方算法迭代计算均方误差函数,同时结合误差函数均方差以及互相关峰值,从而能够自适应场景变化.所提出的算法充分利用相邻多帧之间的相关性,对模拟和实际红外图像序列非均匀性的校正效果突出.实验结果表明本方法能够精确估计非均匀性参数,收敛速度较快,几乎不残留鬼影.

关 键 词:红外焦平面阵列;非均匀性校正;最小均方;多帧配准

中图分类号:TN911.73 **文献标识码**:A

Introduction

Infrared focal-plane arrays (IRFPAs) have been widely used in infrared imaging systems in recent years. However, a FPA suffers from an undesired fixed-pattern noise (FPN) owing to the nonuniformity

Received date: 2013-04-30, **revised date**: 2014-02-19 **收稿日期**:2013-04-30, **修回日期**:2014-02-19

Foundation items: Supported by the Research and Innovation Plan for Graduate Students of Jiangsu Higher Education Institutions, China (CXZZ12_0183), National Natural Science Foundation of China (61101119), Natural Science Foundation of Jiangsu Province of China (BK2011699) and Key Laboratory of Photoelectronic Imaging Technology and System, Beijing Institute of Technology, Ministry of Education of China (2013OEIOF04)

Biography: REN Jian-Le (1987-), Male, Nanjing. PhD candidate. Research interests include infrared image processing, multi-spectral image fusion and multi-view 3D reconstruction

Corresponding author: E-mail: kyleren2010@gmail.com

response of the individual detector when stimulated by the same level of irradiance[1-2]. Moreover, the residual nonuniformity tends to drift slowly and randomly with time when the ambient temperature and other environmental conditions change. Thus, nonuniformity correction (NUC) is a mandatory task for properly calibrating and using several FPA-based cameras.

Numerous NUC techniques have been developed over the years, and it can be divided into two primary categories: 1) reference-based correction using calibrated images on startup and 2) scene-based techniques that continually recalibrate the sensor for parameter drifts. Reference-based corrections using calibrated images on startup cannot solve the drift in the parameters of the detectors over time[3]. The scene-based nonuniformity correction (SBNUC) algorithms are generally identified by two main approaches, namely, statistical methods[4-11] and registration-based methods[12-14]. Algorithms based on statistics assume that all possible values of the true-scene pixel are seen at each pixel location and are described in Ref. [4]. Scribner *et al.* developed a least-mean square based NUC technique that resembles adaptive temporal high-pass filtering of frames[5]. R. C. Hardie *et al.* presented a nouniformity correction method using a modified adaptive LMS algorithm to reduce the update rate at edges within the scene where the "desired" image estimate is the least accurate [8] (GLMS). While this modification significantly reduces ghosting artifacts, it has a slightly longer convergence time. C. Zhang and W. Zhao improved the CS algorithm, and presented the local CS (LCS) algorithm[9]. A PDE-based method that adaptively estimates the gain and the bias using a total variation approach was developed recently by Esteban Vera et al. [10] (TV). The other kind of SBNUC is based on registration. R. C Hardie developed algorithms based on registration require accurate estimation of the motion between frames[13]. Recently, Zuo et al. proposed an improved algorithm based on interframe registration[14] (IRLMS). However, with the changing of scene, the assumption is not satisfied and those methods' performance is unsatisfactory in terms of the balance between convergence speed and ghosting artifacts.

To develop a simple and effective NUC method, we proposed a novel adaptive scene-based nonuniformity correction method based on multiframe registration. It estimates global translation between several adjacent frames, and the resulting mean square error function is optimized by making use of the least mean square (LMS) algorithm. In the learning process of parameter estimation, the local spatial variance of the error function and the value of the correlation peak are considered, which yields a faster and reliable convergence with scarcely ghosting artifacts.

The remainder of this paper is organized as follows. In Section 1 we present the nonuniformity observation model and address our algorithm. Compared experiments are presented in Section 2. Finally, the conclusions of the paper are summarized in Section 3.

1 Scene based nonuniformity correction

In this section, we describe the proposed NUC algorithm in detail.

1.1 Nonuniformity observation model

We assume a linear detector response and model the nonuniformity of each detector with a gain and a bias. At any given frame $n(n=1,2,3,\cdots)$, for each $(i,j)th$ detector in the FPA, the output value $Y_n(i,j)$ is given by

$$Y_n(i,j) = G_n(i,j) \cdot X_n(i,j) + O_n(i,j) \quad (1)$$
$$(i \in [1,M]; j \in [1,N])$$

where the variable $G_n(i,j)$ represents the gain of the $(i,j)th$ detector and $O_n(i,j)$ is the offset of the detector. $X_n(i,j)$ stands for the real incident infrared photon flux collected by the respective detector. M and N are the row and column parameters associated to the FPA, respectively.

NUC is performed by applying a linear mapping to the observed pixel values to provide an estimate of the true scene value so that the detectors appear to be performing uniformly. This correction is given by

$$X_n(i,j) = w_n(i,j) \cdot Y_n(i,j) + b_n(i,j) \quad (2)$$

where $w_n(i,j)$ and $b_n(i,j)$ are, respectively, the gain and offset of the linear correction model of the $(i,j)th$ detector of frame n. Their relation with the real gain and offset could be represented by

$$w_n(i,j) = \frac{1}{G_n(i,j)} \quad , \quad (3)$$

$$b_n(i,j) = -\frac{O_n(i,j)}{G_n(i,j)} \quad . \quad (4)$$

Once the $w_n(i,j)$ and $b_n(i,j)$ are estimated, the nonuniformity parameters $G_n(i,j)$ and $O_n(i,j)$ can be obtained. Therefore, the nonuniformity correction is completed.

1.2 SBNUC using the multiframe registration

Here, if we capture n frames using an $M \times N$ pixel image sensor, the ideal pixel intensity value at (i,j), can be expressed in terms of ideal pixel intensity at $(i+d_y(n), j+d_x(n))$ of frame $(n-t)$ as

$$X_n(i,j) = X_{n-t}(i+d_y(n,t), j+d_x(n,t)) \quad t \in [1,T] \quad ,(5)$$

where $d_y(n,t)$ and $d_x(n,t)$ represent the perpendicular displacement and the horizontal displacement of frame n as against frame $(n-t)$. T is known as the number of adjacent frames. $X_{n-t}(i+d_y(n,t), j+d_x(n,t))$ stands for the real incident infrared photon flux collected by the $(i+d_y(n,t), j+d_x(n,t))th$ detector of frame $(n-t)$. Here, we assume that the level of nonuniformity is not too high, a fairly accurate registration can be performed in the case of global motion. And the registration algorithm used in this paper is a phase correlation algorithm, which can achieve subpixel accuracy[15-16] (shown in Fig. 1)

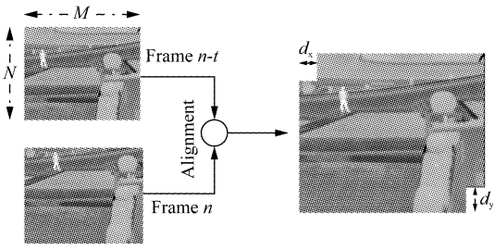

Fig. 1 Diagram of the alignment of the frame n and frame $(n-t)$
图1 第 n 帧和第$(n-t)$帧的匹配框图

From the above discussion, as mentioned in IRLMS method, we firstly define the error function

$$E_{n,t}(i,j) = \hat{Y}_n(i,j) - \hat{Y}_{n-t}(i+d_y(n,t), j+d_x(n,t)) \quad t \in [1,T] \quad ,(6)$$

where $\hat{Y}_n(i,j)$ is corrected value. The error function is defined as the corresponding difference between the two adjacent corrected frames. Therefore in this paper Eq. (6) is defined as

$$E_n(i,j) = \sum_{t\in[1,T]} E_{n,t}(i,j) = \sum_{t\in[1,T]} [\hat{Y}_n(i,j) - \hat{Y}_{n-t}(i+d_y(n,t), j+d_x(n,t))] \quad .(7)$$

To minimize the error $E_n(i,j)$ in the mean square error sense, a functional $e(i,j)$ is defined as

$$e(i,j) = \sum_n E_n^2(i,j) = \sum_n \sum_{t\in[1,T]} [\hat{Y}_n(i,j) - \hat{Y}_{n-t}(i+d_y(n,t), j+d_x(n,t))]^2 \quad ,(8)$$

where the correction parameters $w_n(i,j)$ and $b_n(i,j)$ must be recursively updated in order to minimize the cost function equation (Eq. 8) that allows good NUC performance. Here, we using a stochastic gradient-descent strategy over frames, the correcting parameters $w_n(i,j)$ and $b_n(i,j)$ can be updated as

$$w_n(i,j) = \begin{cases} w_{n-1}(i,j) + \alpha \cdot E_{n-1}(i,j) \cdot Y_{n-1}(i,j) \\ when\ pixel(i,j)\ is\ in\ the\ overlapped\ area \\ w_{n-1}(i,j) \\ else \end{cases} \quad ,(9)$$

$$b_n(i,j) = \begin{cases} b_{n-1}(i,j) + \alpha \cdot E_{n-1}(i,j) \\ when\ pixel(i,j)\ is\ in\ the\ overlapped\ area \\ b_{n-1}(i,j) \\ else \end{cases} \quad ,(10)$$

where the parameter α is known as the learning rate. It should be pointed out that the correction parameters are only updated in the overlapped part between frame $(n-t)$ and frame n. We initialize the learning rate of the gain and bias corrections with $w_1(i,j) = 1$ and $b_1(i,j) = 0$. Note that to obtain good convergence, we have found it necessary to scale the input data to lie within the interval $[0,1]$. This allows the gain and offset to converge with a common step size.

Several methods which are based on registration[12-14] assume that the temperature field of the observed scene does not change during several adjacent frames. However, if the objects in the scene are not motionless, this assumption cannot be met well so that real scene may leak into the error signal. To overcome this weakness, a spatially adaptive LMS approach has been proposed in Ref. 8 that adjust the convergence rate based on local spatial variance of the observed image. In addition, the presence of registration errors may make the matter even worse. Thus, based on the knowledge that the local spatial

average of error function has advantage act on the learning rate, the proposed adaptive learning rate is designed to be dependent, and inversely proportional to the local spatial variance centered at pixel (i,j) of the error function $\sigma^2_{E_n(i,j)}$. Thus, the learning rate α can be written as

$$\alpha = K \cdot \frac{1}{1 + \sigma^2_{E_n(i,j)}} \quad . \quad (11)$$

Therefore, if the error function has a high local spatial variance, then the error of adjacent frames is less confident, and the learning rate gets smaller value. The updating of the correction coefficients is halted when the incoming value has a higher local spatial variance, where K is a constant that regulates the maximum learning rate allowed. The local spatial variance $\sigma^2_{E_n(i,j)}$ can be calculated with any desired window size. However, a 3×3 window size will be assumed in this paper. This mechanism prevents biased estimates from improper updating caused by the outliers and helps to sample data better.

From the above discussion, it is obvious that the learning rate α represents the step size of the algorithm and governs the convergence speed. The proposed method is based on multiframe registration, the registration accuracy is crucial to the correction parameter estimation. The used registration algorithm is mentioned in Section 1.2 which depends on phase correlation peak corresponding to the true shift. The value of the phase correlation peak is a direct indicator that shows whether two images could be well aligned. And we add the peak value to the learning rate.

$$\alpha = K \cdot \frac{1}{1 + \sigma^2_{E_n(i,j)}} \cdot c_{\max} \quad , \quad (12)$$

where $c_{\max}$ denotes the value of the phase correlation peak corresponding to the true shift. When the brightness along the motion trajectory is not constant and there is rotation between two adjacent frames, small value of peak is obtained easily. At the same time, small values of α is recommended.

2 Experimental results

In this section, we compare the various SBNUC algorithms, such as TV, LCS, GLMS and IRLMS, and in particular demonstrate the efficacy of the proposed algorithm. And a number of experimental results are presented.

The infrared sequences with artificial nonuniformity are generated from a clear 300 frame infrared video sequence, which was collected at 11 am by using a 320×256 HgCdTe FPA camera operating in the $3 \sim 5$ μm range and working at 50 FPS. And the corrupted video sequences are obtained by using a synthetic gain with a unit-mean Gaussian distribution with standard deviation of 0.1, and a synthetic offset with a zero-mean Gaussian distribution with standard deviation of 30.

The GLMS algorithm was tested with a step size of 0.05 and $T = 20$ and two window sizes of 3×3 for an average filter and 21×21 for a Gaussian low-pass filter as suggested in Ref. 8. In IRLMS, the learning rate α takes the value of 0.05 and update trigger displacement was set to 3.5 (recommended in Ref. 14). In the MRA-NUC algorithm, a set of 5 frames was registered ($T = 5$) and update trigger displacement was set to 3.5 too. Subpixel registration was performed[15-16], and the alignment was done with bilinear interpolation. The metric used to measure the NUC performance is given by the root-mean square error (RMSE), which is defined as

$$\mathrm{RMSE} = \sqrt{\frac{\sum_{i=1}^{M}\sum_{j=1}^{N}[\hat{Y}(i,j) - Y(i,j)]^2}{M * N}} \quad , (13)$$

where $Y(i,j)$ is the $(i,j)th$ pixel's value of the true frame, while $\hat{Y}(i,j)$ is the pixel's value of the corrected frame. $M * N$ denotes the size of image.

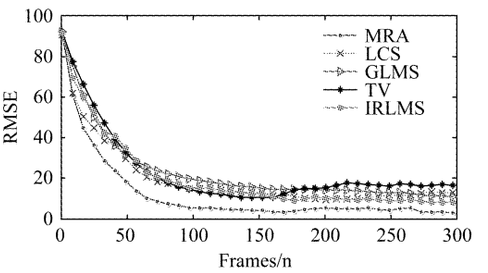

Fig. 2　RMSE results of the nonuniformity correction using different methods
图 2　不同非均匀性校正方法的 RMSE 结果

It can be observed from Fig. 2 that the RMSE of MRA-NUC algorithm can be reduced below 20 within

50 frames. The RMSE for GLMS decreases as fast as IRLMS, but MRA-NUC presents a consistent decrease of around 20% over TV, GLMS and IRLMS for the first 150 frames, and then it keeps decreasing and reaches a gap of nearly 5 over IRLMS. In addition, MRA-NUC reports the smallest values of RMSE and has a fast convergence speed and stability with hardly rebound.

An image sample of the correction results of simulated nonuniformity image sequence is shown in Fig. 3. Figure 3(a) shows the image for the 140th frame with synthetic nonuniformity. The outputs using TV, LCS, GLMS, IRLMS and MRA-NUC are shown in Fig. 3 (b)-3(f), respectively. It can be observed from Fig. 3(b-d) that some residual nonuniformity and ghosting artifacts can be perceived. Moreover, the correction result which relates to the original image became blurred. From Fig. 3(e), the level of residual nonuniformity is low. However, we can barely see any ghosting artifact and residual nonuniformity in the MRA-NUC result. Through a naked-eye evaluation, the ability of MRA-NUC for compensation for the FPN promptly is clearly seen.

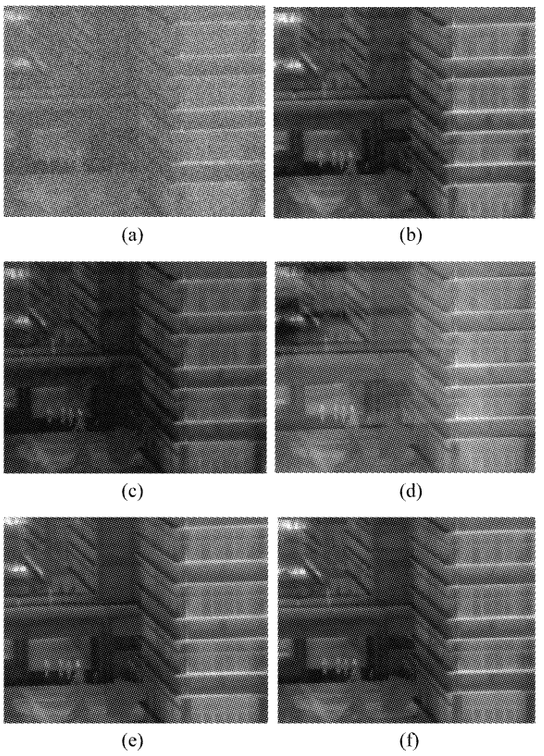

Fig. 3 Correction with simulated nonuniformity images using different methods (Frame 140th) (a) Image with simulated gain and offset nonuniformity, (b) corrected result with TV. (c), corrected result with LCS, (d) corrected result with GLMS, (e) corrected result with IRLMS, (f) corrected result with MRA-NUC

图3 模拟非均匀性不同方法的校正结果(140帧)(a) 含有模拟增益和偏置非均匀性的图像,(b) TV方法校正结果,(c) LCS方法校正结果,(d) GLMS方法校正结果,(e) IRLMS方法校正结果,(f) MRA-NUC方法校正结果

In the following subsection, we test the proposed algorithm with real infrared data, which is acquired by a 320×256 HgCdTe FPA camera operating in the 8 ~ 14 μm range and at a rate of 50 FPS in a tall building. A sample frame of the test sequence is shown in Fig. 4. When we testing NUC in real infrared images, and apart from the naked-eye evaluation, it hardly obtains the calibration data needed to perform a radiometrically accurate correction used as a reference for comparison purposes, only the roughness index(ρ), which measures the high-pass content of an image, is of used[10,14]. The NUC over the real IR data sequence using the selected parameters with above is shown in Fig. 4. The results for the average roughness values obtained for each algorithm are presented in Table 1. From there, the MRA-NUC obviously outperformed all the other NUC algorithms in the mean sense.

表1 实际IR数据的Mean Roughness结果

Table 1 Mean roughness ($\rho \times 10^{-3}$) results for the real IR data sequence

不同算法	Roughness $\rho(\times 10^{-3})$
原始数据	1.844
TV	1.597
LCS	1.622
GLMS	1.578
IRLMS	1.213
MRA-NUC	1.104

Sample image from the video sequence is shown in Fig. 4(a). The corrected results using the five different algorithms are shown in Fig. 4(b)-4(d). It is obvious that the nonuniformity presented in the raw frame has been notably reduced by all the NUC methods. The GLMS algorithm, a 3 × 3 spatial average kernel is probably too small to smooth the nonuniformity effectively, leading to a much slower convergence rate than IRLMS method. Besides, in the output of the TV, LCS and GLMS, some low spatial frequency residual nonuniformity are clearly visible. The MRA-NUC method,

in contrast, converges faster, and it obtains better result in contrast to others methods. Comparison and analysis of the outputs of the five different methods show that MRA-NUC is almost without residual nonuniformity, and hardly ghosting artifact could be detected. It has been presented to be superior to the existing methods and can achieve excellent NUC results with small computational load.

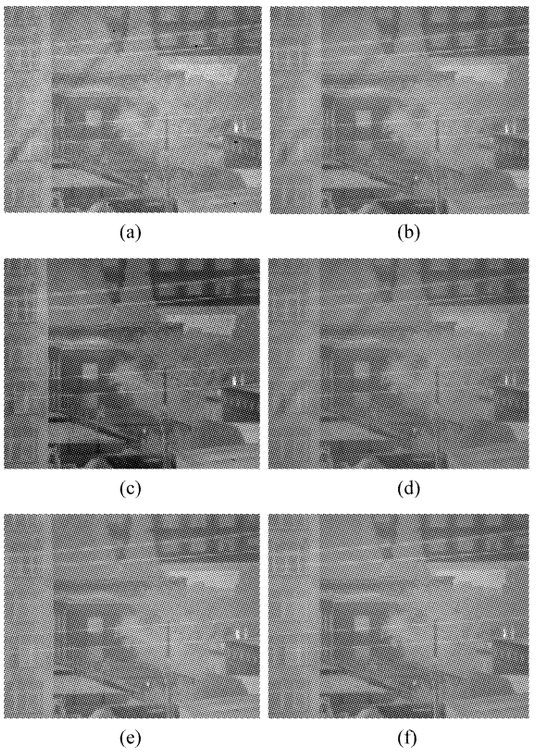

Fig. 4 Correction with raw infrared images with real nonuniformity using different methods (Frame 60th) (a) Sample image from the video sequence, (b) corrected result with TV, (c) corrected result with LCS, (d) corrected result with GLMS, (e) corrected result with IRLMS, (f) corrected result with MRA-NUC
图 4 实际含非均匀性的红外图像校正结果(60 帧)(a)视频序列的一帧,(b) TV 方法校正结果,(c) LCS 方法校正结果,(d) GLMS 方法校正结果,(e) IRLMS 方法校正结果,(f) MRA-NUC 方法校正结果

From the above discussion, we can easily conclude that the proposed method has the best NUC performance. To demonstrate the potential advantages of using an adaptive learning rate for the mulitiframe based NUC method for all kinds of complicated scenes, we have selected an output frame of the same real infrared image sequence containing a local moving target that seriously deviate from global translation between several adjacent frames. The results are shown in Fig. 5. IRLMS was proved to be effective compared with GLMS and MCA. We conclude that IRLMS makes the best performance in the several NUC methods to some extent. Therefore, we only gave the results corrected with IRLMS and MRA-NUC. In fact, there are some local moving people/car in Fig. 5 with slow speed. However significant change in a local region (i. e. ghosting artifact) is invisible to naked eye. Figure 5 (a)-5(b) show the results corrected with IRLMS and MRA-NUC respectively. Figure 5(c)-5(d) show the estimated offset parameter corrected with IRLMS and MRA-NUC respectively. Based on the estimation of global translation between adjacent frames, a constant parameter was adopted in IRLMS. However, there are some local moving targets in the true scene, a constant parameter is inapplicable.

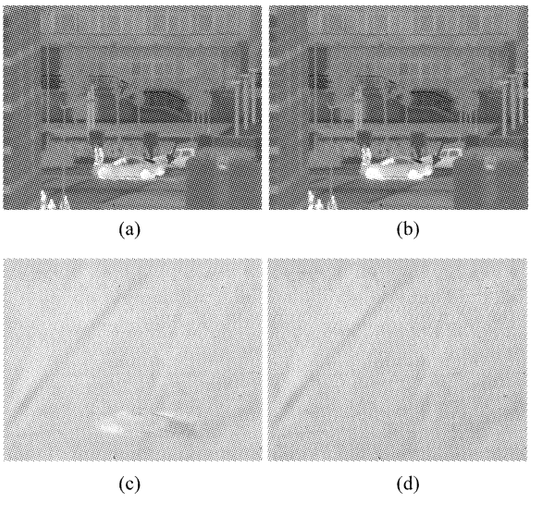

Fig. 5 Correction with raw infrared images with two different methods (a) Corrected result with IRLMS, (b) corrected result with MRA-NUC, (c) estimated offset parameter with IRLMS, (d) estimated offset parameter with MRA-NUC
图 5 实际红外图像两种不同方法的校正结果(a) IRLMS 方法校正结果,(b) MRA-NUC 方法校正结果,(c) IRLMS 方法偏置参数的估计,(d) MRA-NUC 方法偏置参数的估计

From Fig. 5 we can see that a moving car in the bottom of the sample frame. With the motion of camera, the car also moves at its own speed. The static image "burns" into the correction parameters, and as the motion continues, the residual moving car is still visi-

ble superimposed on the new "corrected" scene. Note that the proposed method has significantly reduced artifact. This is because the local spatial variance of error function was calculated to prevent the residual moving scene from burning in. To explain more clearly, local amplification results are shown in Fig. 6. Obvious ghosting artifact is clear for all to see in Fig. 6(a). The above experimental results demonstrate MRA-NUC's great performance and capabilities to avoid undesirable effects.

(a) (b)

Fig. 6 Local amplification results (a) Corrected result with IRLMS, (b) Corrected result with MRA-NUC
图6 局部放大结果(a) IRLMS 方法校正结果,(b) MRA-NUC 方法校正结果

3 Conclusions

We have presented a novel scene-based nonuniformity correction method for fixed-pattern noise removal based on multiframe registration. The method adopts a phase-correlation method to estimate the global translation between several adjacent frames. To achieve the gain and offset correction parameters of the FPA, we used an LMS algorithm to minimize the mean square error. In the presented experimental results, we have shown that when local motion exists, MRA-NUC can be properly control the update process along with the changing of all kinds of complicated scenes. In addition, we compared our algorithm with TV, LCS, GLMS and IRLMS methods, which represent perhaps the most commonly employed statistical method and registration-based method. In short, the proposed algorithm has shown its superiority to nonuniformity correction for it greatly reduces the ghosting artifacts and almost no residual nonuniformity. What's more, the algorithm can be easily implemented in hardware for real-time processing.

REFERENCES

[1] Scribner D A, Kruer M, Killiany J. Infrared focal plane array technology[J], *Proc. IEEE*. 1991,**79**: 66-85.

[2] Schulz M, Caldwell L. Nonuniformity correction and correctability of infrared focal plane arrays[J], *Proc. SPIE*. 1995,**2470**: 200-211.

[3] Friedenberg A, Goldbatt I. Nonuniformity two-point linear correction errors in infrared focal plane arrays[J], *Opt. Eng*. 1998,**37**: 1251-1253.

[4] Harris J G, Chiang Y M. Nonuniformity correction of infrared image sequence using the constant-statistics constraint [J], *IEEE Trans, Image Proc*. 1999,**8**: 1148-1151.

[5] Scribner D A, Sarkady K, Caulfield J T. *et al*, Nonuniformity correction for staring focal plane arrays using scene-based techniques[J], *Proc. SPIE*. 1990, **1308**: 224-233.

[6] Qian W X, Chen Q, Bai J, *et al*. Adaptive convergence nonuniformity correction algorithm[J], *App. Opt*. 2011, **50**: 1-10(2011).

[7] Torres S N, Hayat M M. Kalman filtering for adaptive nonuniformity correction in infrared focal plane arrays[J], *J. Opt. Soc. Am. A*, 2003,**20**: 470-480.

[8] Hardie R, Baxley F, Brys B., *et al*. Scene-based nonuniformity correction with reduced ghosting using a gated LMS algorithm[J], *Opt. Express* 2009,**17**: 14918-14933.

[9] Zhang C, Zhao W. Scene-based nonuniformity correction using local constant statistics[J], *J. Opt. Soc. Am. A*, 2008,**25**: 1444-1453.

[10] Vera E, Meza P, Torres S. Total variation approach for adaptive nonuniformity correction in focal-plane arrays[J], *Opt. Lett*. 2011,**36**: 172-174.

[11] Ren J, Chen Q, Qian W, *et al*. Efficient single image stripe nonuniformity correction method for infrared focal plane arrays[J], *Opt. Rev*. 2012,**19**: 355-357.

[12] Hardie R C, Hayat M M.. Scene-based nonuniformity correction using video sequences and registration[J], *Appl. Opt*. 2000,**39**: 1241-1250.

[13] Ratliff B M, Hayat M M, Hardie R C. An algebraic algorithm for nonuniformity correction in focal-plane arrays [J], *J. Opt. Soc. Am. A* 2002,**19**: 1737-1747.

[14] Zuo C, Chen Q, Gu G, *et al*. Scene-based nonuniformity correction algorithm based on interframe registration[J], *J. Opt. Soc. Am. A*, 2011,**28**: 1164-1176.

[15] Kuglin C D, Hines D C. The phase correlation image alignment method[J], *Proceeding of the International Conference of the Cybernetics Society*, 1975: 163-165.

[16] Guizar-Sicairos M, Thurman S T, Fienup J. R. Efficient subpixel mage registration algorithms [J], *Opt. Lett*. 2008,**33**: 156-158.